Optimization of an Environmental-Friendly Ranque-Hilsch Vortex Tube Energy System by Means of CFD Simulation in Order to Produce Sustainable Energy

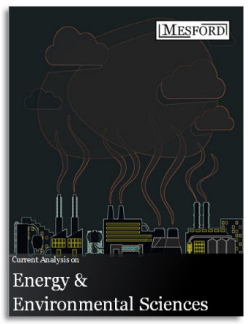

Ali Heydari[a], Adib Bazgir [b], Mohammad shahibzadeh[c], Nader Nabhani[d,*]

[a,b]*Petroleum University of technology, Department of Gas Engineering, Ahwaz, Iran.*
[c]*AmirKabir University of technology (Tehran polytechnic), Mahshahr Campus, Department of chemical Engineering, Mahshahr, Iran.*
[d]*Petroleum University of technology, Department of Mechanical Engineering, Ahwaz, Iran.*

Abstract:

A vortex tube is a mechanical device which significantly separates the inlet gas stream into hot and cold streams and therefore provides a variety of environmentally-friendly applications such as steam production and cooling. Due to the absence of chemicals or electrical parts, there is no harmful influence on the atmosphere or environment and thus can be utilized in different industries. The vortex tube is simulated with 1, 3 and 5 fins installed on hot-tube using six different geometries in order to increase the efficiency of clean energy production for both cooling and heating purposes. The result of the research is then compared with prior experimental results brought in literature. This article surveys the influence of different fin shapes on critical performance parameters of cold temperature difference (ΔT_c), the hot temperature difference (ΔT_h), isentropic efficiency and COP aiming toward producing clean energy. The modeling results indicate that the 5 triangular fins and 3 square fins have the highest and lowest cold temperature difference (ΔT_c), isentropic efficiency and COP, respectively.

Publication History: Received: 22 October 2018 | Revised: 11 December 2018 |Accepted: 24 December 2018

Keywords:
Ranque-Hilsch Vortex Tube; Environmental-friendly energy production; Clean Energy; Numerical simulation (CFD); Thermal efficiency; shape of fins; number of fins.

1. INTRODUCTION

Ranque-Hilsch Vortex Tube is a mechanical device which is commonly used in refrigeration and cooling operations. However, it is applicable for both refrigeration and heating purposes. A Vortex Tube can be utilized to produce steam for industrial applications in absence of inlet work, or it might be used in spot-cooling without of using chemicals and thus can be very applicable in environmentally-friendly processes. It has been subjected of interest for many years and therefore it can be replaced with variety of industrial devices that contaminate the environment and in consequence, climate change can be prevented dramatically. When it comes to efficiency, it is most rewarding to use vortex tube instead of any device for cooling, heating or steam production which magnificently supports energy saving due to no work input requirement. They are usually used for inexpensive cooling when pressurized air is accessible. The device mainly consists of the following parts: inlet nozzle(s), vortex chamber, hot conical valve, hot outlet, and cold outlet. Sometimes a diffuser is also installed between the cylindrical tube outlet and the hot valve. High-velocity helical motion of air stream is mostly made by tangential inlet nozzle. The entered gas is separated into a cold and hot stream, which exit through the cold end and the opposite hot tube respectively. Pressurized gas is injected tangentially into a swirl chamber and accelerated to a high rate of rotation. Due to the conical nozzle at the end of the tube, only the outer shell of the compressed gas is allowed to escape at the hot end. The remainder of the gas which has lower temperature is forced to return in an inner vortex of less diameter within the outer vortex flow and exits through the cold outlet. The invention belongs to Ranque, a metallurgist and physicist [1] in 1933. At that time, it was declared to be thermodynamically inefficient and since it is experimentally investigated and optimized by Hilsch [2], this mechanical device is named as Ranque-Hilsch vortex tube (RHTV).

*Address correspondence to this author at Petroleum University of Technology, Department of Mechanical Engineering Ahwaz, Iran.; Tel: +989163060189; E-mail: Nabhani@put.ac.ir

Mesford Publisher Inc
Office Address: Suite 2205, 350 Webb Drive, Mississauga, ON L5B3W4, Canada; T: +1 (647) 7109849 | E: caee@mesford.ca, contact@mesford.ca, https://mesford.ca/journals/caee/

The clean energy prior discussions and energy separation within a vortex tube (also known as Ranque-Hilsch Effect) is discussed in this presentation. Among researchers on clean energy, Edwards et al. [3] examined the challenges facing hydrogen and fuel cell technology that must be solved in order to significantly increase the efficiency of fuel cells for more energy production. Momirlan and Veziroglu [4] presented the benefits of hydrogen combustion and current pollutants and the transition of changing from fossil fuels to clean hydrogen energy. Pant et al. [5] discussed recent developments of Bio-electrochemical systems in order to produce sustainable energy using organic wastes and industrial wastewaters aiming to replace them with conventional fuel cells. Poizot and Dolhem [6] investigated non-CO2 producing energy sources, economics and issues for electrochemical energy production and storage focusing on lithium-ion technology. Srirangan et al. [7] reviewed the most recent and future challenges in the development of biomass and transformation technologies for clean production of biofuels.

The Vortex tube is a promising source of energy production for both heating and cooling purposes since it is a more efficient, environmental-friendly, accessible and cheap device to produce clean energy with an absence of chemicals or work input. Smith Eiamsa-ard and Pongjet Promvonge [8] and Subudhi and Sen [9] provided extensive reviews of performed experiment researches on vortex tube. There were researchers who also examined the simulation of turbulence inside vortex tube using different models by Ansys fluent software. The simulation of vortex tube and turbulent vortex flow inside it is very difficult due to complex and compressible flow structure. Eiamsa-ard and Promvonge and Sharma et al. [8, 10] reviewed numerical examinations of the vortex tube. Behera et al. [11] and analyzed thermal and flow pattern inside the vortex tube applying CFD code. Aljuwayhel et al. [12] applied a CFD simulation to investigate the physical separation process and results indicated a good prediction of the applied a numerical model in energy separation. Eiamsa-ard and Promvonge [13] performed numerical investigation to predict the physics of flow pattern and energy separation inside the device. Farouk and Farouk [14] used a large eddy simulation (LES) approach to show temperature distribution inside a vortex tube. They also compared different inlet gases such as nitrogen and helium on flow behavior [15]. Last recently, Liu et al. [16] reported their effort considering the effect of compressibility of fluids and swirl characteristics using CFD simulation.

This paper applies numerical simulation to predict flow behavior and temperature distribution within the device to study the influence of different fin shapes and a number of fins on the refrigeration performance thus can provide an approach to replace this device with other common environment contaminating sources of energy. As far as authors are concerned, such simulation about the effect of fins on vortex tube performance parameters is novel. The result is then verified by means of comparison with the results of previously conducted experiments. Then the numerical model is used to survey the effect of internal fin installation on performance efficiency of the device. For an analogy, the information for the vortex tubes with 1, 3 and 5 fins (triangle, square, rectangle, circle, parallelogram and trapezium) carried out under the same operating condition. due to a higher effeciency of five fins on the hydrodynamics of flow pattern, only contours and streamlines of vortex tubes with 5 fins along hot-tube are illustrated in results.

2. STRUCTURE OF THE GEOMETRY AND GRID INDEPENDENCE STUDY

Fig. (**1**) shows the schematic of the hot-tube structure and grid with different shapes of utilized fins which are installed on the inner surface of hot-tube. Characteristics of the simulated counter-flow vortex tube and applied fins which have same geometric dimensions are also shown in Fig. (**1**) (e.g. fin position, fin dimensions, etc). The design condition is the same as applied by Liu *et al.* [16]. The variation of temperature difference of cold tube against cold flow ratio with various quantities of cells is brought in table 1 in order to reduce error related to unmapped grids. The diversity of cases 6 and 7 in cold mass ratio and the temperature difference of cold is not greater than 1%. It was observed that for above 400,000 grid cells, no remarkable increase in cold flow ratio and the temperature difference of cold was observed with regard to a refinement of inlet and outlets. Therefore, case 6 is considered as the basic mesh for this research.

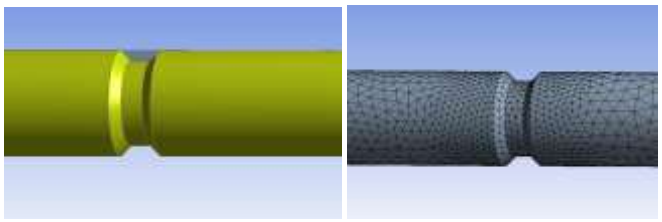

Figure 1(a) Trapezium fin.

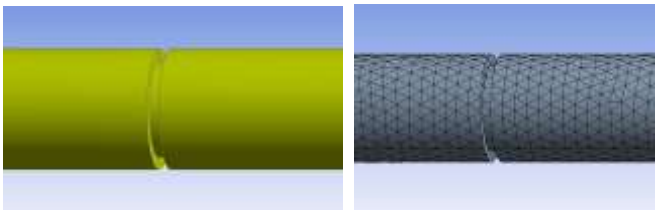

Figure 1(b) Square fin.

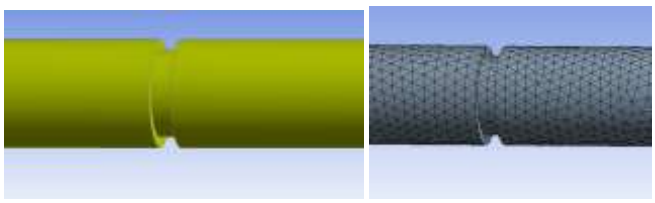

Figure 1(c). Rectangular fin.

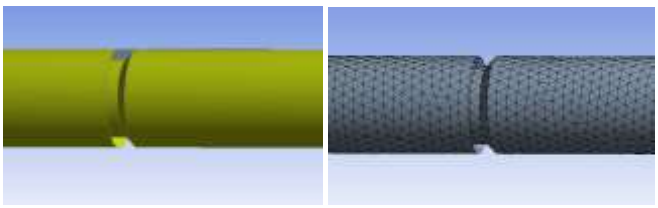

Figure 1(d) Parallelogram fin.

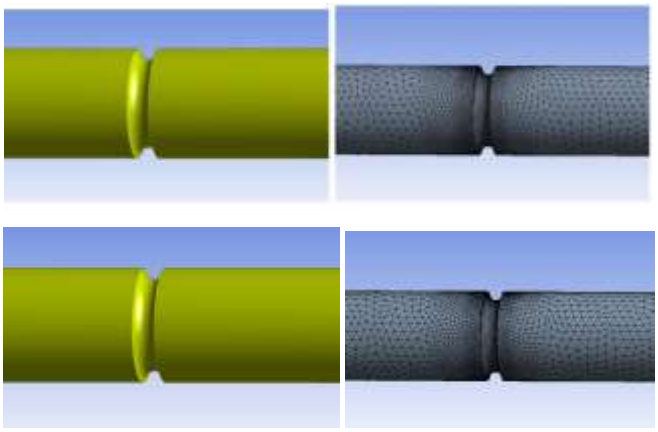

Figure 1(e) Circular fin.

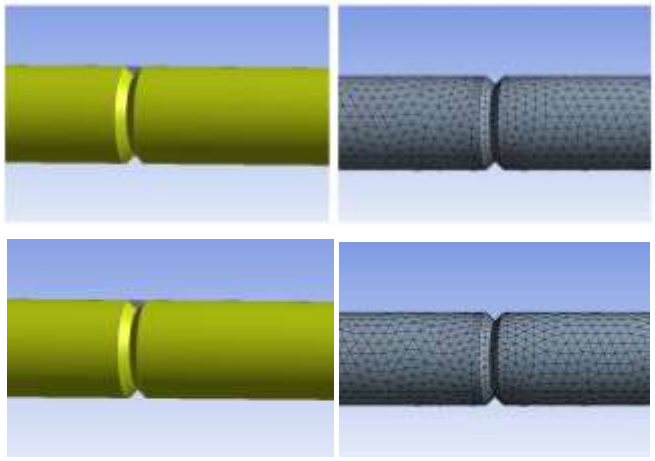

Figure 1(f) Triangular fin.

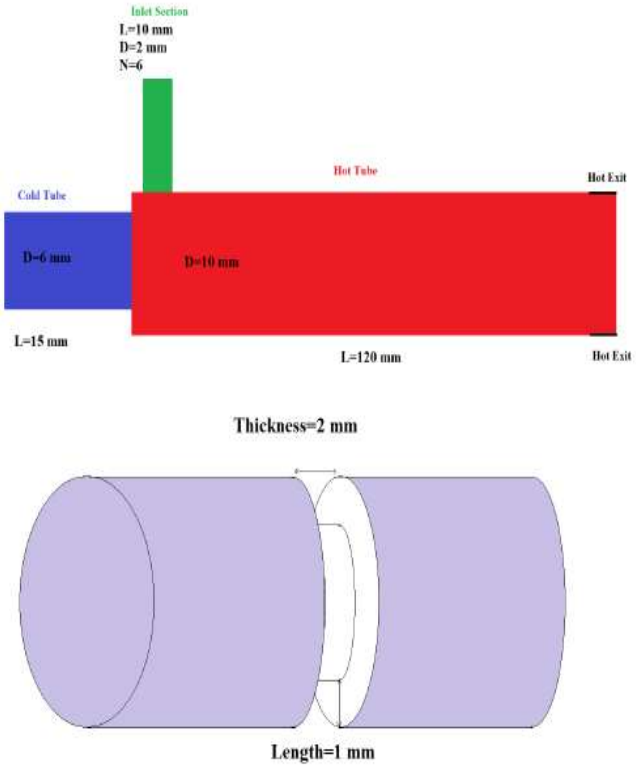

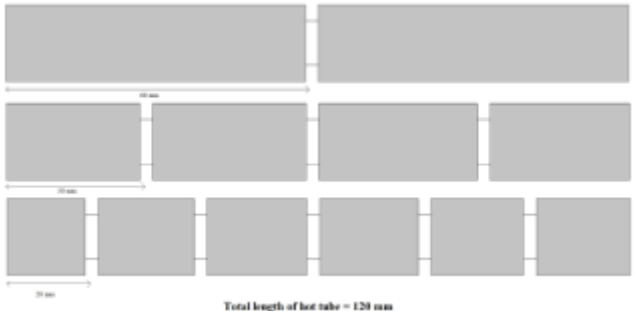

Figure 1(g) dimensions of simulated vortex tube and applied fins.

Figure 1 Geometry and mesh grid of fins.

3. PARAMETRIC STUDY

The terms below are used as parameters to justify the effectiveness of vortex tube:

Pressure loss ratio:

$$\lambda = \frac{\Delta P_c}{P_{in}} = \frac{P_{in} - P_c}{P_{in}} \quad (1)$$

Where Pin (Pa) is absolute pressure of inlet flow and Pc (Pa) is absolute pressure of the cold outlet.

Cold mass ratio:

$$\xi = \frac{\dot{m}_c}{\dot{m}_{in}} \quad (2)$$

Where m_c (kg / S) is the mass flow rate of the cold air, and m_{in} (kg / S) is the mass flow rate of the inlet air.

Cold temperature difference:

Cold temperature difference presents the refrigeration performance which is defined as:

$$\Delta T_c = T_{in} - T_c \quad (3)$$

Where T_{in} (K) is the temperature of inlet and T_c (K) is temperature of cold outlet.

Hot temperature diminution:

$$\Delta T_H = T_H - T_{in} \quad (4)$$

Where Tin (K) is the total temperature of air at the air intake and T_x (K) is the total temperature of air at hot exit.

Isentropic efficiency:

The isentropic efficiency for the air with isentropic expansion within RHVT is defined as below [8]:

$$\eta_{is} = \frac{\Delta T_c}{\Delta T_{is}} = \frac{T_{in} - T_c}{T_{in}\left(1 - {P_a}/{P_{in}}\right)^{\frac{\gamma-1}{\gamma}}} \quad (5)$$

In which $\eta_{is}, \Delta T_{is}(K), P_{in}(bar), P_a$ and γ are considered the isentropic efficiency, isentropic temperature difference, inlet air pressure, ambient pressure and ratio of specific heat, respectively.

Coefficient of performance:

Considering the principle of ideal gas isentropic expansion, the coefficient of performance (COP) can be formulated[8]:

$$cop = \frac{Q_c}{W} = \frac{\alpha C_p (T_{in} - T_c)}{(\frac{\gamma}{\gamma - 1}) RT_{in} [(^{p_{in}}/_{p_c})^{\frac{\gamma-1}{\gamma}} - 1]} \quad (6)$$

Where Q_c is the cooling rate and W is the mechanical energy spent for cooling of the inlet air.

4. NUMERICAL MODELING

4.1. Problem Details

A vortex tube with same characteristics of Liu *et al.* [16] is simulated and studied. Working fluid is compressible, turbulent and steady state. The aim is to determine the effect of fins inside hot tube on temperature Separation. The software applied for the simulation is ansys 16.2 to deploy the present modeling. Fig. (**2**) clearly shows that increase in pressure loss ratio results in increase of temperature difference between cold and hot tube. This verifies that temperature separation within vortex tube is directly caused by pressure loss ratio and larger pressure loss ratio results in increment of temperature separation. Fig. (**2**) also indicates that both modeling and experimental results of Liu et al. [16] and current 3-D model totally verify each other, which verifies present numerical model and solution method to be reliable. Such states bolds the fact that current numerical model is a sufficient approach for discovering temperature separation and general dynamics inside the vortex tube.

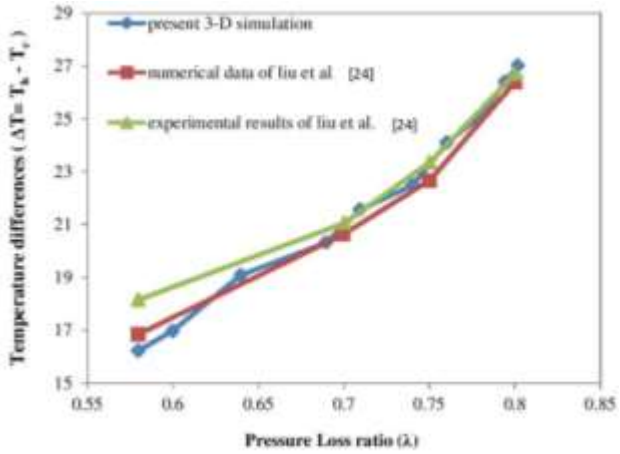

Figure 2 Experimental and numerical variation of total ($\Delta T = T_h - T_c$) temperature difference with pressure loss ratio (λ).

4.2. Governing Equations

The characteristics of compressible swirl flow within the device are calculated by solving conservation equations of mass, momentum and energy. The RNG k-ε turbulence code is represented to solve the flow complexity. The whole formulas are mentioned below [16]:

Continuity equation:

$$\frac{\partial}{\partial x_i}(\rho u_i) = 0 \quad (7)$$

Momentum equation:

$$\frac{\partial}{\partial x_i}(\rho u_i u_j) = -\frac{\partial p}{\partial x_i} + \frac{\partial}{\partial x_j}\left[\mu\left(\frac{\partial u_i}{\partial x_j} + \frac{\partial u_i}{\partial x_i} - \frac{2}{3}\delta_{ij}\frac{\partial u_l}{\partial x_l}\right)\right] + \frac{\partial}{\partial x_j}(-\rho\bar{u}_i\bar{u}_j) \quad (8)$$

Energy equation:

$$\frac{\partial}{\partial x_i}[u_i(\rho E + p)] = \frac{\partial}{\partial x_j}\left[\left(K_e + \frac{c_p\mu_t}{Pr_t}\right)\frac{\partial T}{\partial x_j} + u_i(\tau_{ij})_{eff}\right] + S_h \quad (9)$$

Viscous dissipation $(\tau_{ij})_{eff}$ is defined as below:

$$(\tau_{ij})_{eff} = \mu_{eff}\left(\frac{\partial u_j}{\partial x_i} + \frac{\partial u_i}{\partial x_j}\right) - \frac{2}{3}\mu_{eff}\frac{\partial u_k}{\partial x_k}\delta_{ij} \quad (10)$$

Ideal gas equation:

$$P = \rho RT$$

using Boussinesq assumption [17] to bond the Reynolds stress:

$$-\rho\bar{u}_i\bar{u}_j = \mu_t\left(\frac{\partial u_i}{\partial x_j} + \frac{\partial u_j}{\partial x_i}\right) - \frac{2}{3}\left(\rho k + \mu_t\frac{\partial u_k}{\partial x_k}\right)\delta_{ij}$$

The RNG k-ε turbulence model is derived using Navier-Stokes formulas, applying a mathematical progress that is known as renormalization group (RNG) approaches. In excess, extended details and explanations of RNG principle and its applications to turbulent flow can be studied in reference [18]. formulas below are Transport formulas for RNG k-ε model:

$$\frac{\partial}{\partial x_i}(\rho k u_i) = \frac{\partial}{\partial x_j}\left(\alpha_k\mu_{eff}\frac{\partial k}{\partial x_j}\right) + G_k + \rho\varepsilon - Y_M \quad (13)$$

$$\frac{\partial}{\partial x_i}(\rho\varepsilon u_i) = \frac{\partial}{\partial x_j}\left(\alpha_\varepsilon\mu_{eff}\frac{\partial \varepsilon}{\partial x_j}\right) + C_{1\varepsilon}\frac{\varepsilon}{k}G_k - C^*_{2\varepsilon}\rho\frac{\varepsilon^2}{k} \quad (14)$$

The effective viscosity is acquired by:

$$d\left(\frac{\rho^2 k}{\sqrt{\varepsilon\mu}}\right) = 1.72\frac{\hat{v}}{\sqrt{\hat{v}^3 - 1 + C_v}}d\hat{v} \quad , \quad \hat{v} = {}^{\mu_{eff}}/_{\mu} \quad , \quad C_v \approx 100 \quad (15)$$

$$C^*_{2\varepsilon} = C_{2\varepsilon} + \frac{C_\mu\eta^3(1 - \frac{\eta}{\eta_0})}{1 + \beta\eta^3} \quad (16)$$

$$\eta = (2S_{ij}.S_{ij})^{1/2}.\frac{k}{\varepsilon} \quad (17)$$

$$S_{ij} = \left(\frac{\partial u_i}{\partial x_j} + \frac{\partial u_j}{\partial x_i}\right) \quad (18)$$

Eq. (11) is modulated to gain an exacting description of effect of variation of turbulent transport and Reynolds number (or eddy scale) on each other.

Explanation of generation of turbulence kinetic energy is calculated:

$$G_k = -\rho\bar{u}_i\bar{u}_j\frac{\partial u_i}{\partial x_i} \quad (19)$$

The dilatation dissipation term, Y_M, is contained in equation k. This term is coded based on a suggestion by Sarkar [19]:

$$Y_M = 2\rho\varepsilon Ma_t^2 \quad , \quad Ma_t = \sqrt{\frac{k}{\gamma RT}} \quad (20)$$

The model constants are:

$C_\mu = 0.0845, C_{1\varepsilon} = 1.44, C_{2\varepsilon} = 1.44, \alpha_k = \alpha_\varepsilon = 1.39, Pr_t = 0.85, \beta = 0.012$

More information is included in reference [17] about details of governing equations and RNG k-ε code.

4.3. Solution Scheme and Boundary Conditions

RNG k-ε CFD code is utilized to simulate current research article. The governing equations for this analysis are solved deploying finite volume method. For convective-diffusive terms in the (RANS) equations, continuity and momentum equations, the energy equations, second order upwind (SOU) scheme are gathered with RNG k-ε turbulence model equation [20] are deployed. SIMPLE is also selected for Pressure-Velocity. The simulation is solved by Intel CORE ™ i7 system, 3 GHz Processor and 12 GB RAM (DDR3). Simulation aims to investigate the stream pattern, temperature, velocity behavior and density and pressure distributions of the presented simulations. Due to the complex flow geometry scheme, boundary conditions are based on experimental results by Liu et al. [16], as follows:

4.3.1. Inlet

Compressed air reaches the device tangentially via intake nozzles. Experimental researches usually prepare inlet information as inlet pressure (P_{in}), inlet temperature (T_{in}) and mass flow rate of inlet $(\dot{m}_{in})$ for an inlet nozzles. In the current simulation, inlet pressure is assumed to be 0.3-0.4 MPa and inlet temperature is assumed as 300 K.

4.3.2. Wall

Walls are considered stationary, adiabatic and no slip.

4.3.3. Outlets

Cold tube and hot tube outlets are considered pressure outlet giving the pressure value in the range of 0.08 and 0.18 MPa respectively.

5. RESULTS AND DISCUSSION

5.1. Velocity Components and Flow Behavior

Three-dimensional pattern of velocity for straight Ranque-Hilsch tube along the hot-tube with different fin shapes is shown. Due to the small value of radial and axial velocities, only total and tangential velocity values and streamlines of the device with different fin shapes are shown in Fig. (**3**) respectively. For total pressure of P_in=0.3 MPa, P_c= 0.08 MPa and P_h= 0.18 MPa (all values are absolute), the highest total velocity is approximately 320 m.s-1 into inlet nozzle region and decreases steeply to zero near the walls. The tangential or swirl velocity, which is more than the axial and radial velocities, is the substantial velocity component inside the device. The tangential velocity is strongly affected by tangential shear stress near the wall. Tangential velocity magnitude approximately equals to inlet velocity, which decreases as the fluid flows from inlet zone to hot tube, also noticing that the tangential component is increased in the radial direction, unless at positions very close to the wall.

Analyzing the Fig. (**4**) which illustrates the axial and radial cross-sections of different geometries of fins, velocity $\eta_0 = 4.$ magnitudes of the device for different fin shapes principally differs and this difference is more obvious at the inlet region. As we move further to the hot end, total velocity is quickly reduced and similarly total velocity patterns are observed in all positions. The circular flow pattern is created as the velocity increases at the inlet nozzle, and total pressure decreases in consequence. Considering that the tangential velocity is directly proportional to radial distance, the outer hot stream is a free vortex. The radial component of velocity at various locations shows a free vortex nearby the walls and the component decreases to a significant value at the core region. Very low kinetic energy at the center of vortex tube is the result of minimum total velocity at the central region of the tube. The maximum amount of total velocity that flows at the inlet region is approximately 320 m.s-1. These cross-sections of axial view have the greatest total velocity implanted with triangular fins. Therefore, analysis of total velocities in cross-sections of the device indicates that peripheral flow transforms energy (thermal transformation) and it results from an increase in hot flow temperature and pressure expansion and angular momentum transfer majorly causes temperature drop in the cold outlet. It is also clear that total velocity component equals to zero at the certain radius at core flow. The velocity regions relate to regions of cold and hot flow before and after this radius respectively. Thus, the stagnation point has defined the point in which velocity value reaches zero at core flow. Results illustrate that total velocity at the center of flow is maximum in a device with triangular shaped fins.

5.2 Density and Pressure Profiles

Density and the absolute value of total pressure contours are marked in Fig. 5 for straight vortex tubes for different fin shapes at P_in=0.3 MPa (absolute). Density pattern is similar to pressure due to the ideal gas assumption. These figures obviously show that both the absolute value of total pressure and density obtain the highest value at the inlet section. The minimum value of absolute pressure is approximately 0.06796 MPa for straight vortex tubes with 5 triangular fins respectively from 0.3 MPa at the inlet, whereas maximum velocity grows rapidly to 320 m.s-1 for vortex tubes with 5 triangular fins (Fig. (**5f**)). The density gradient for the vortex tube with 5 triangular fins is more than the other devices. This ranging in density gradient within vortex tube obviously proves the temperature separation. In other words, since the vortex tube with 5 triangular fins obtains greater density gradient with respect to the others; it produces a higher eccentric force, which is the major driving force of energy separation.

5.3 Temperature Profile

The temperature distribution and thermal analysis are required in order to enhance the performance of refrigerator device. The dependence of total temperature to static temperature can be presented by the following equation assuming compressible fluid:

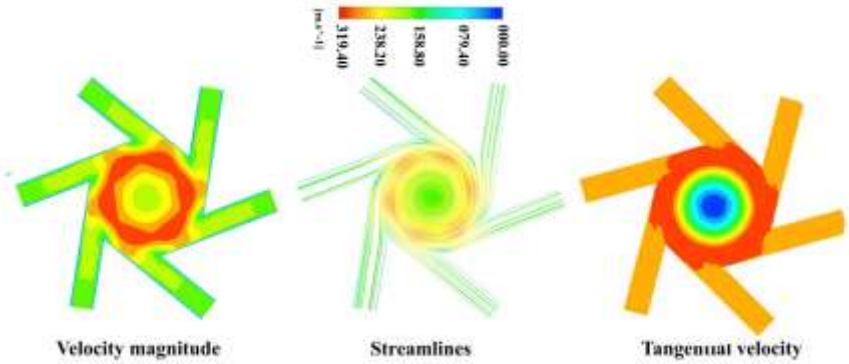

Figure 3(a) five trapezium fins.

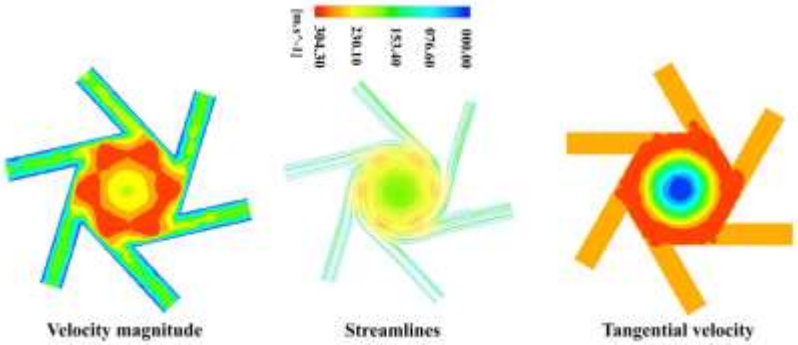

Figure 3(b) five square fins.

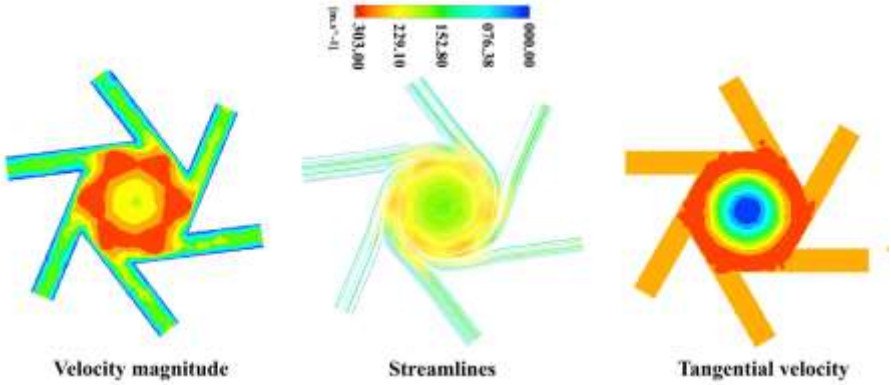

Figure 3(c) five rectangular fins.

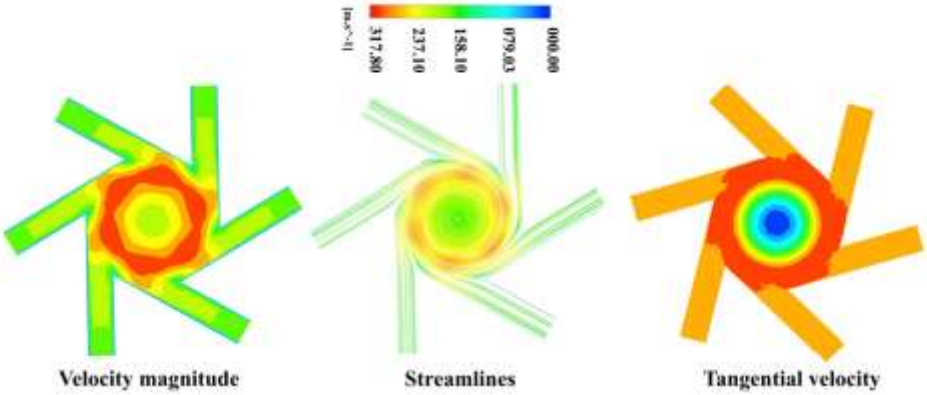

Figure 3(d) five parallelogram fins.

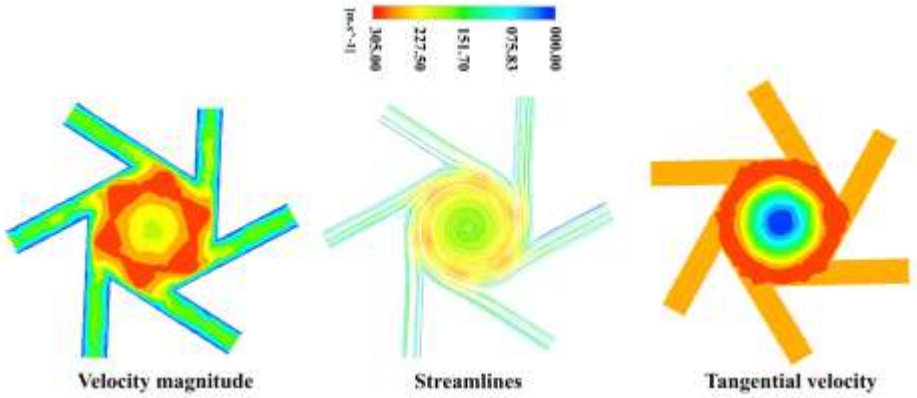

Figure 3(e) five circular fins.

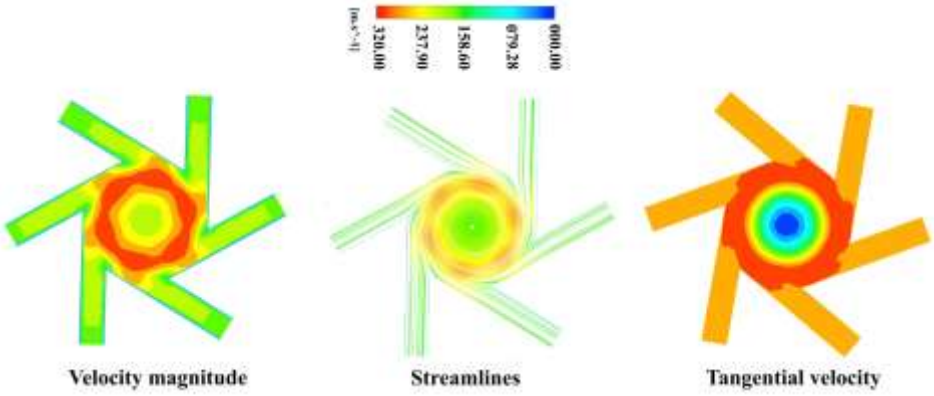

Figure 3(f) five triangular fins.

Figure 3 Velocity profiles.

$$T = T_{st}[1 + \frac{\gamma - 1}{2} Ma^2] \quad (22)$$

In this equation, Ma represents Mach number. Fig. (**6**) illustrates the static and total temperature pattern for vortex tubes for different fin shapes at P_in= 0.3 MPa (absolute). The maximum total temperature is 328.1 K for vortex tubes with 5 rectangular fins, while the minimum value is 246 K for vortex tube with 5 triangular fins. These figures illustrate that the temperature reduction within the device with the 5 triangular fins is higher than the other vortex tubes; moreover, in all sorts of the device the temperature increases unto the hot end while decrease toward the cold end is observed. Static temperature significantly decreases near the intake region due to isentropic expansion. Radial static temperature gradient motivates heat transfer. As Fig. 6 illustrate, in core region the static temperature radially reduces. But due to the no-slip boundary condition, the static temperature suddenly grows near the walls. Heat is transferred from a greater static temperature area to a less static temperature zone and major thermal interplay between the two flow streams occurs between the inlet and the stagnation points.

5.4. Thermal Analysis of Vortex Tubes

According to Fig. (**7a**, **b**), the effect of pressure loss ratio on a temperature difference of hot and cold is brought. The increase in absolute total pressure results in an increase of hot and cold temperature differences. The vortex tube with rectangular fin has a lower cold temperature difference with respect to other fins. At λ=0.66, at constant absolute pressure, a maximum temperature difference of cold exists. For the vortex tube with 5 triangular fins greatest cold temperature difference at P_in= 0.3 MPa is calculated to be 16.7 K as shown in Fig. (**7a**) and for P_in = 0.4 MPa, the greatest cold temperature difference 20.7 K as shown in Fig. (**7b**). The highest hot temperature difference is obtained at λ=0.66. For the vortex tube with 5 rectangular fins, the maximum hot temperature difference at P_in= 0.3 MPa is calculated to be 19.5 K as shown in Fig. (**7**) (b) and for P_in= 0.4 MPa is the maximum hot temperature difference 23.5 K as shown in Fig. (**7b**). For $0.6 < \lambda < 0.78$, the vortex tube with 5 rectangular fins has a greater hot temperature difference than the other ones. Moreover, from these diagrams, the observed trend in coldest temperature in the vortex tube with 5 triangular fins is due to centrifugal force which causes the expansion at the core of the vortex flow which highly dependent on density which directly affecting the centrifugal force.

From Fig. (**8a**, b), it can be seen that if the thickness of cold core increases, the cold temperature difference (〖ΔT〗_C) will increase as well, which will cause an increase in efficiency. The isentropic efficiency of vortex tubes at P_in= 0.3 MPa and P_in= 0.4 MPa are shown in Fig. (**8a**, **b**) respectively. The isentropic efficiency is directly related to the cold temperature

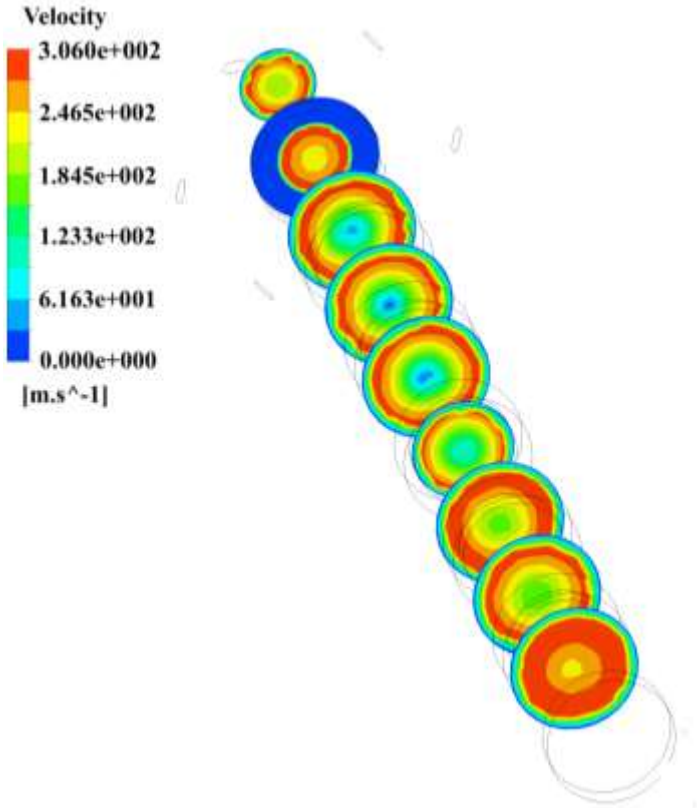

Figure 4(a) five trapezium fins.

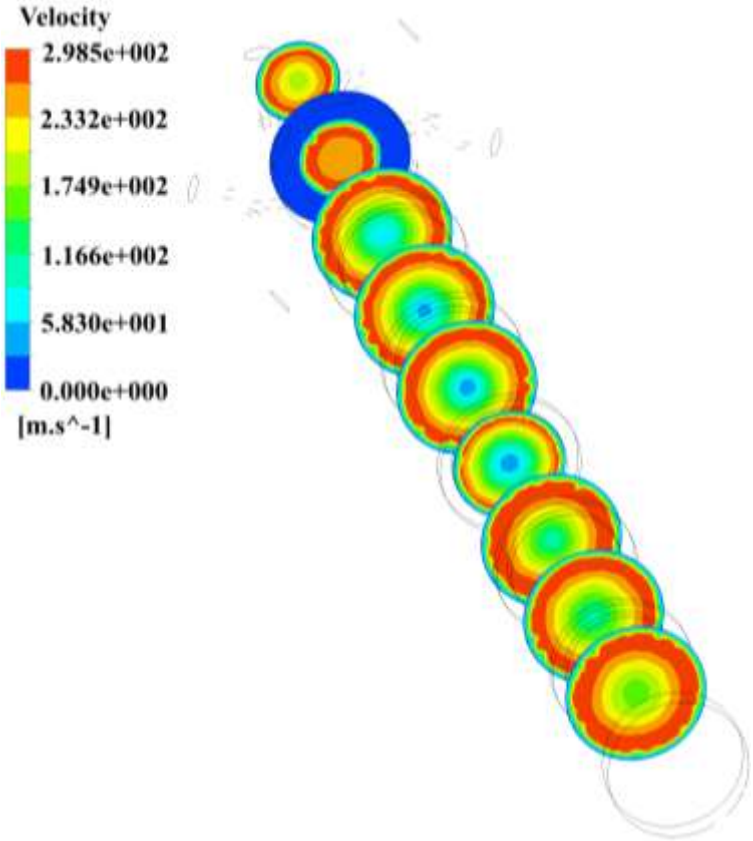

Figure 4(b) five square fins.

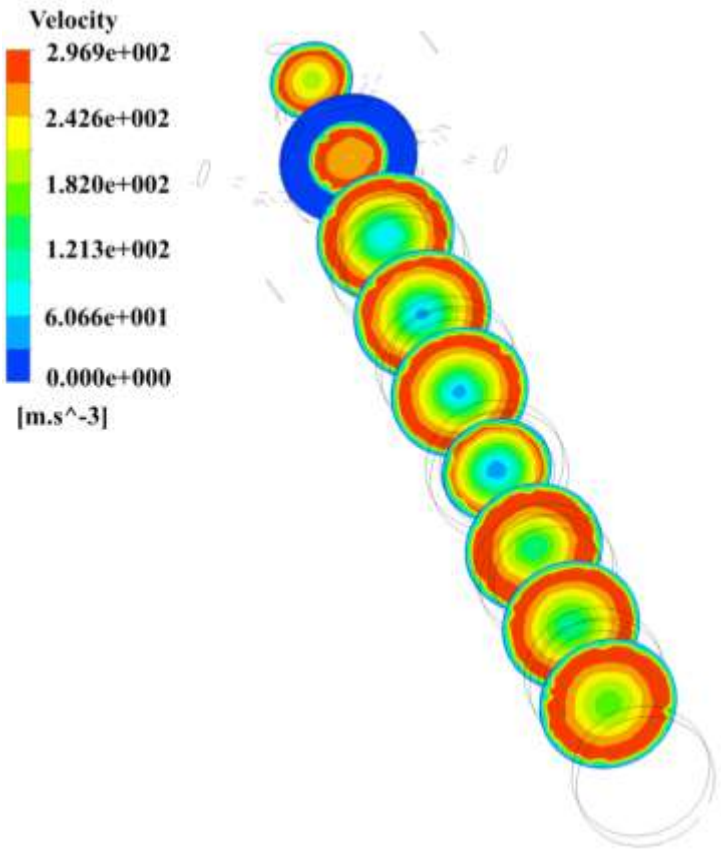

Figure 4(c) five rectangular fins.

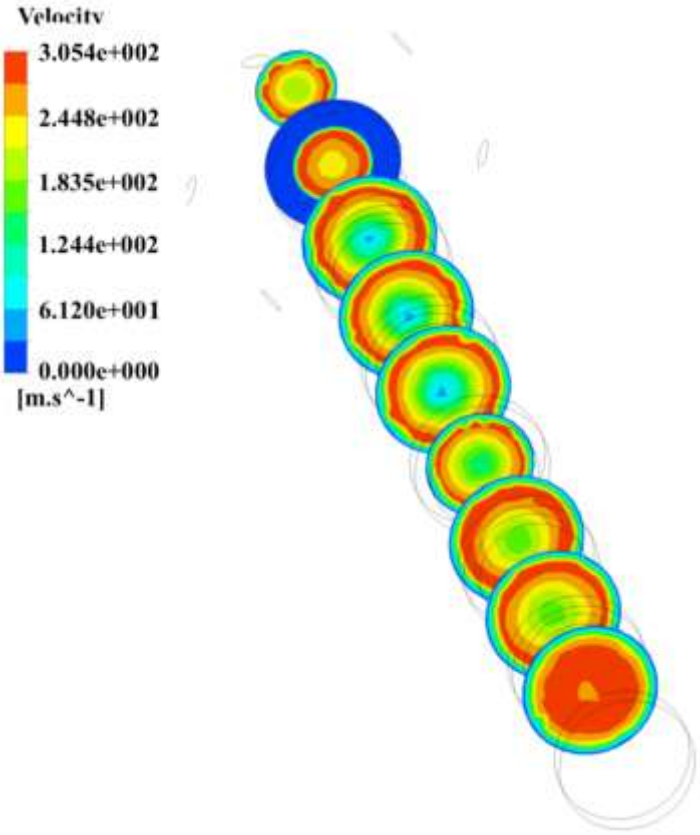

Figure 4(d) five parallelogram fins.

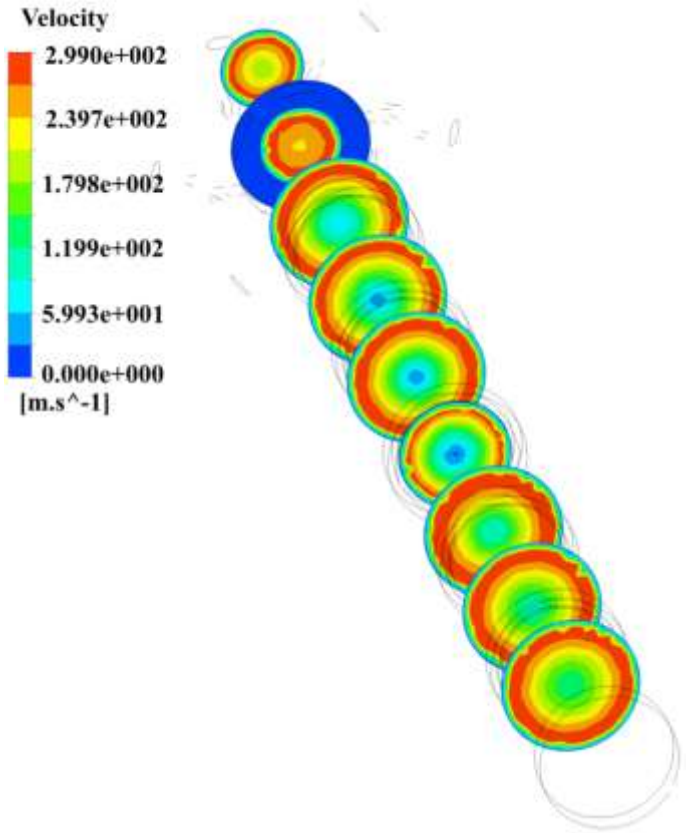

Figure 4(e) five circular fins.

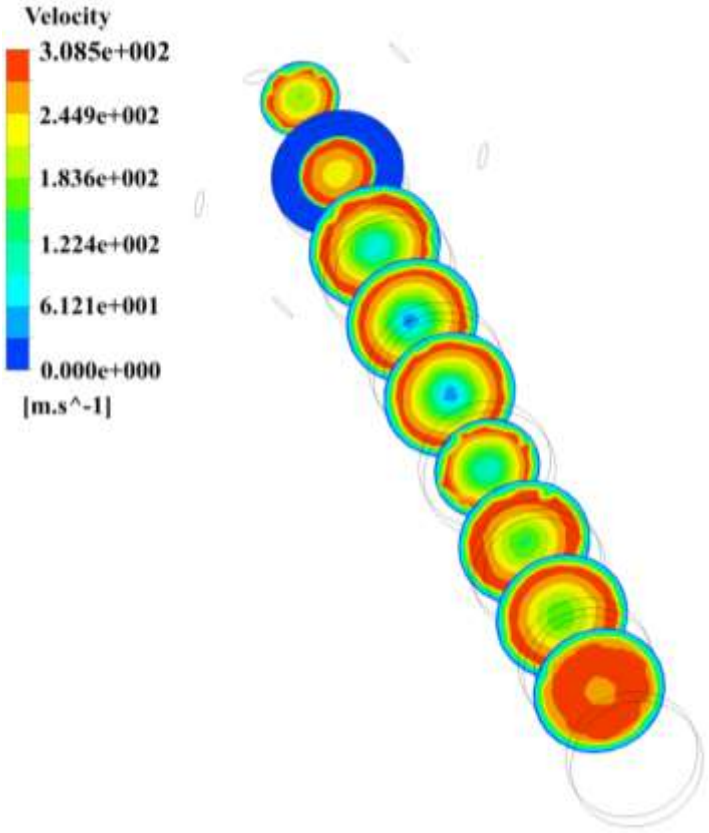

Figure 4(f) five triangular fins.

Figure 4 Velocity profiles along the vortex tube.

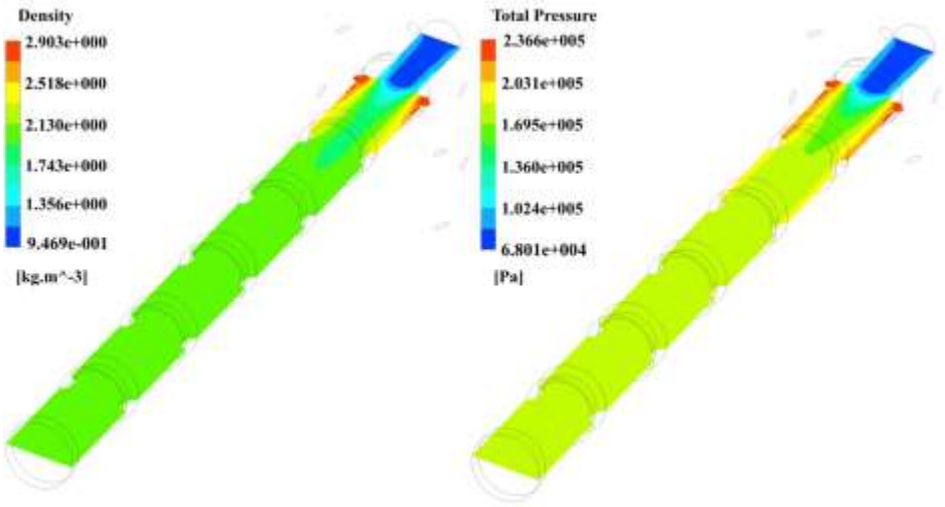

Figure 5(a) five trapezium fins.

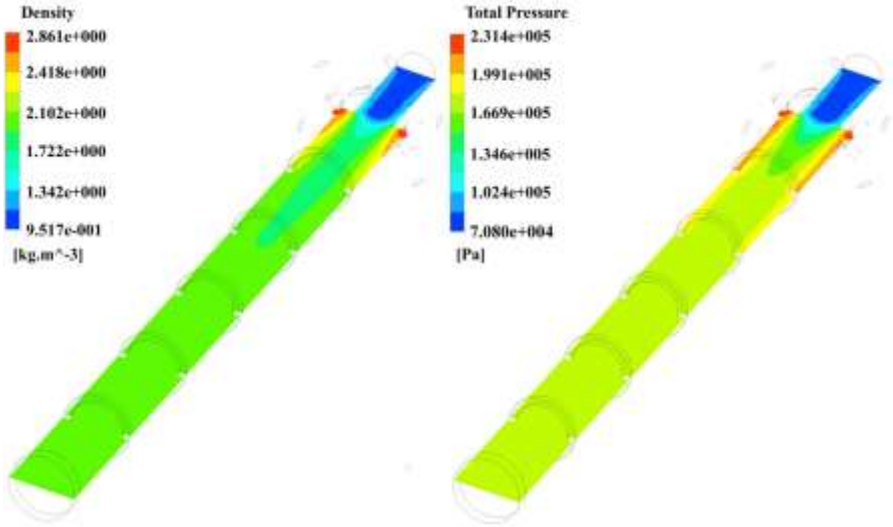

Figure 5(b) five square fins.

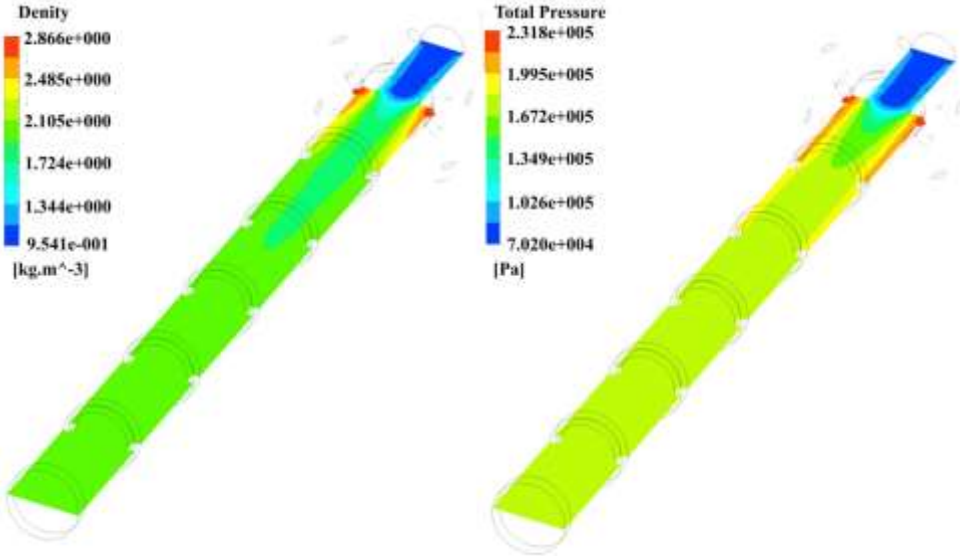

Figure 5(c) five rectangular fins.

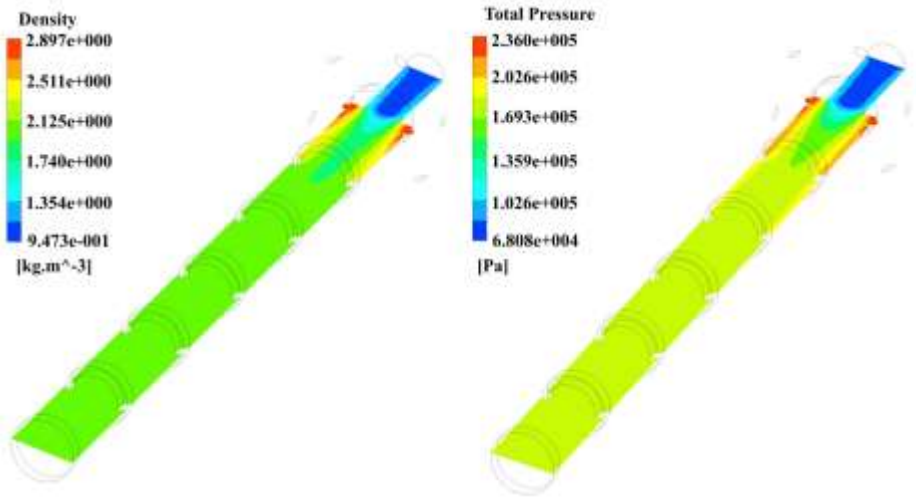

Figure 5(d) five parallelogram fins.

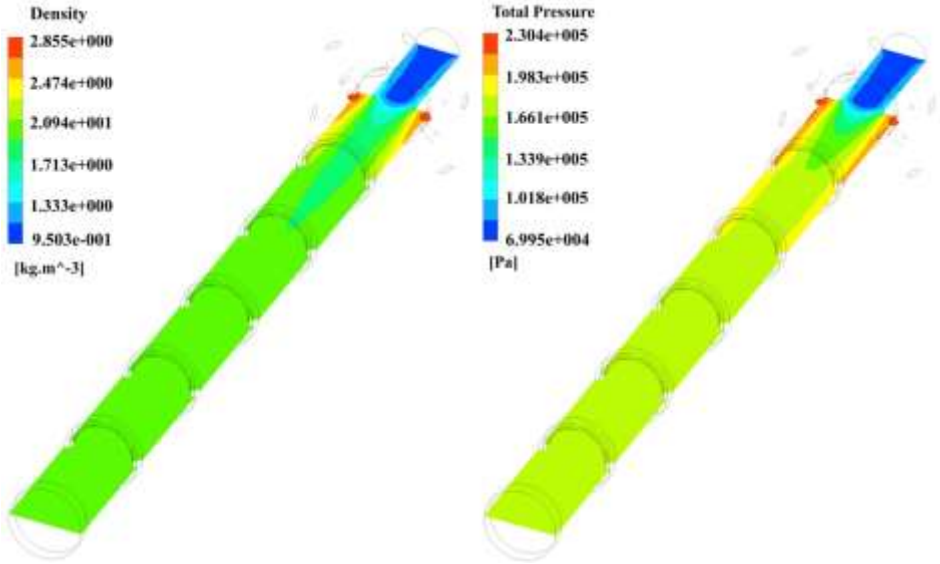

Figure 5(e) five circular fins.

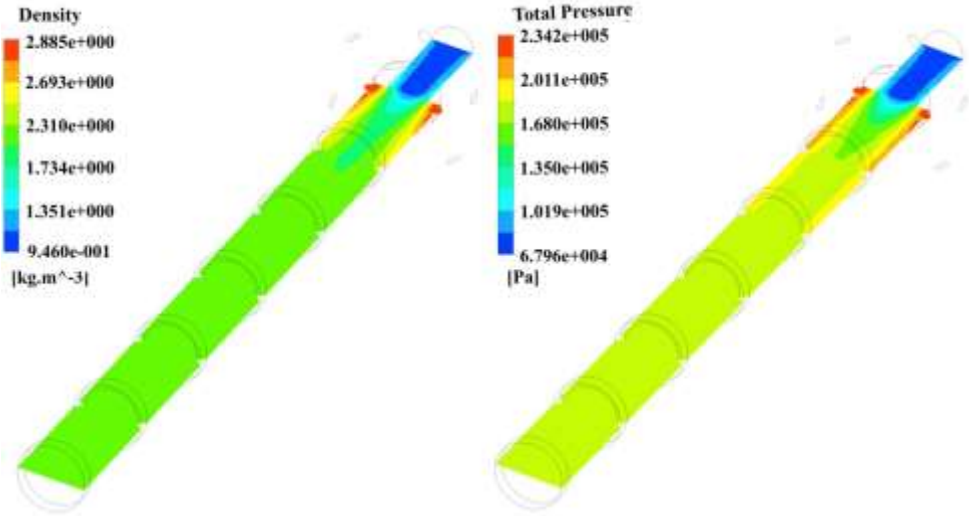

Figure 5(f) five triangular fins.
Figure 5 Density and Pressure profiles.

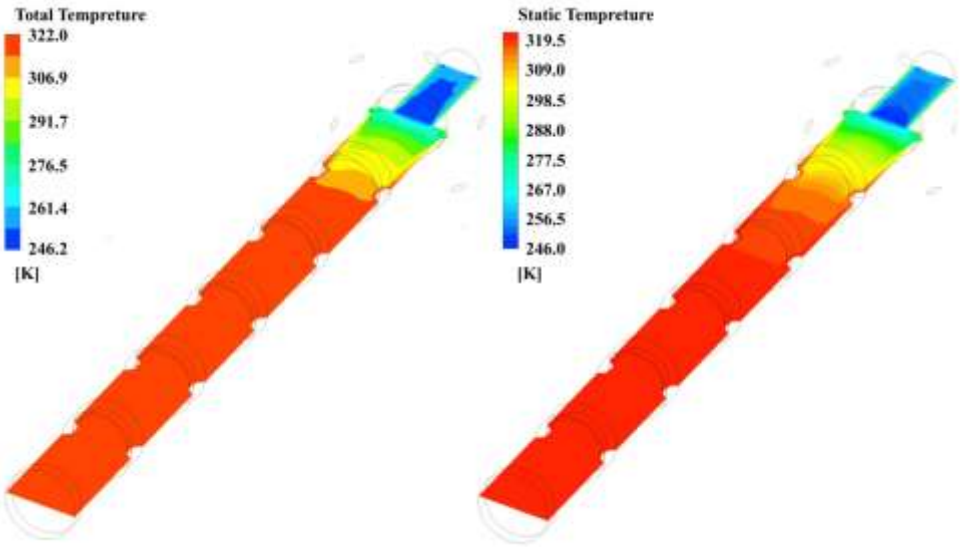

Figure 6(a) five trapezium fins.

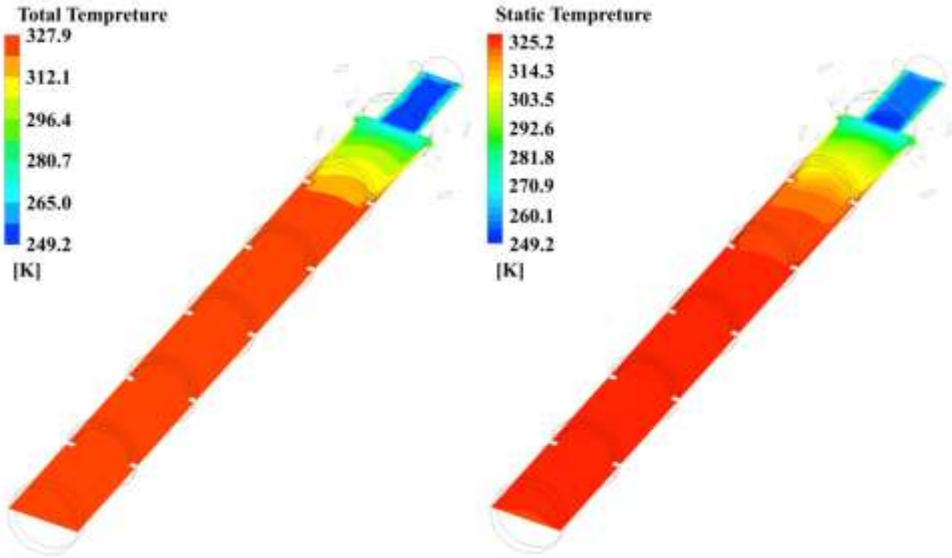

Figure 6(b) five square fins.

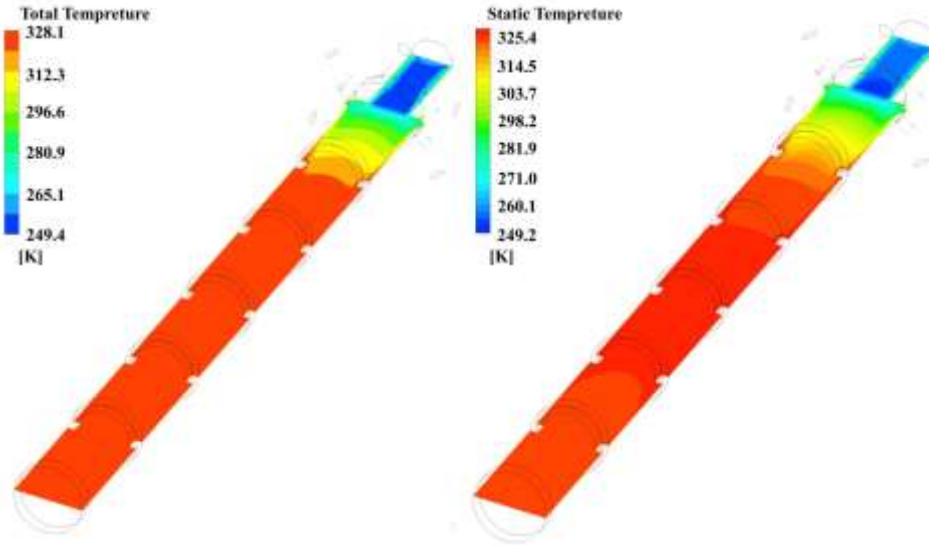

Figure 6(c) five rectangular fins.

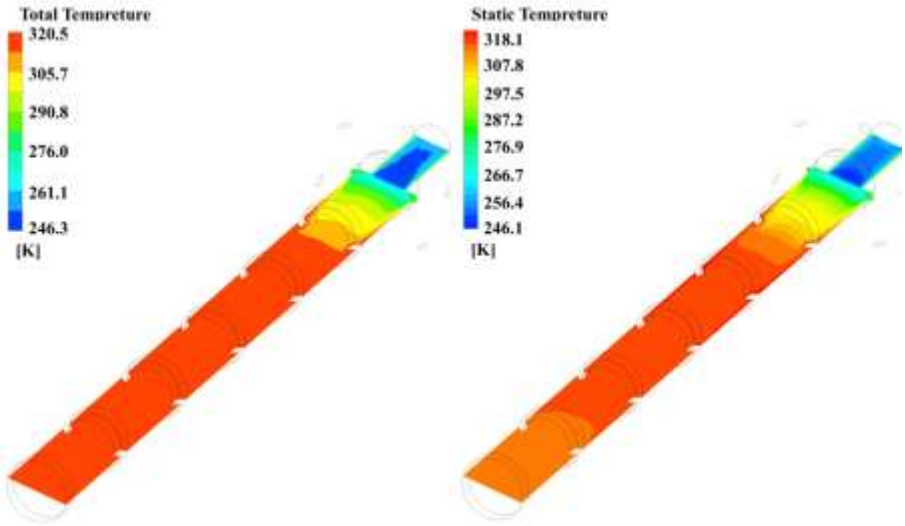

Figure 6(d) five parallelogram fins.

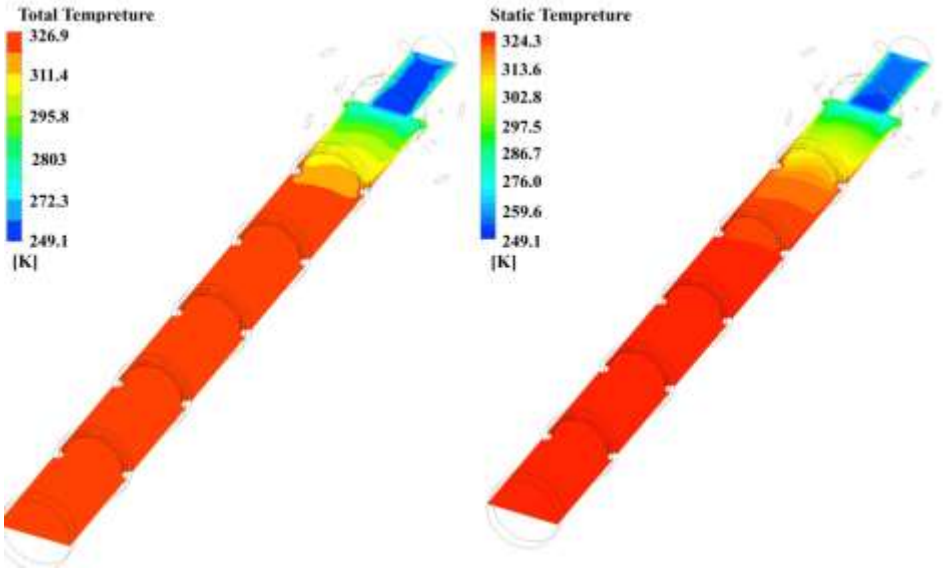

Figure 6(e) five circular fins.

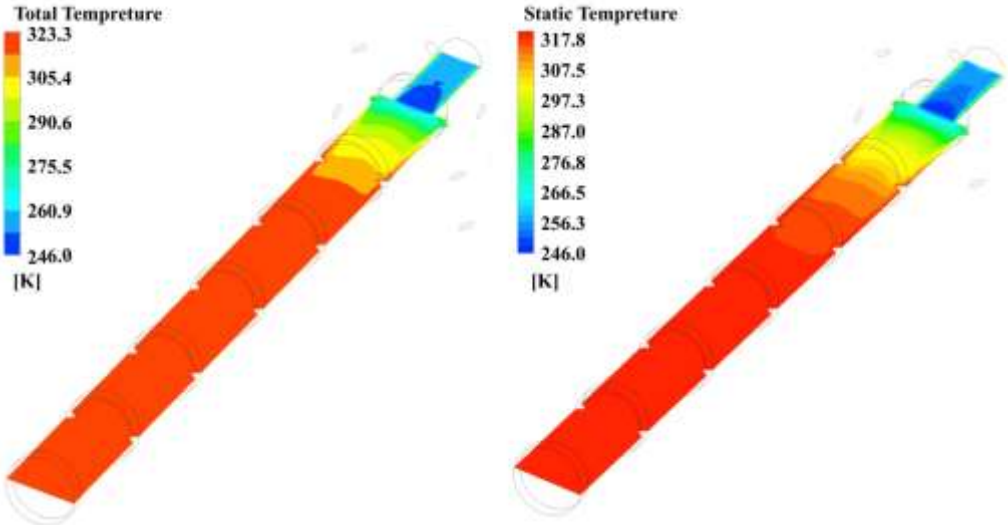

Figure 6(f) five triangular fins.

Figure 6 Total and Static temperature profiles.

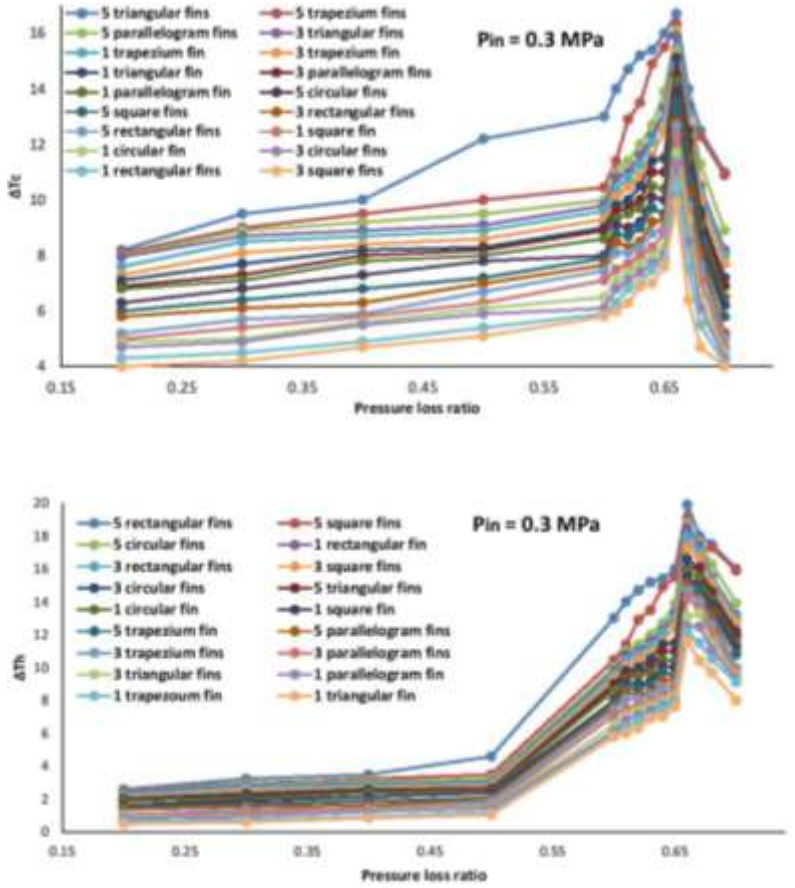

Figure 7 (a) cold and hot temperature difference at Pin = 0.3 MPa

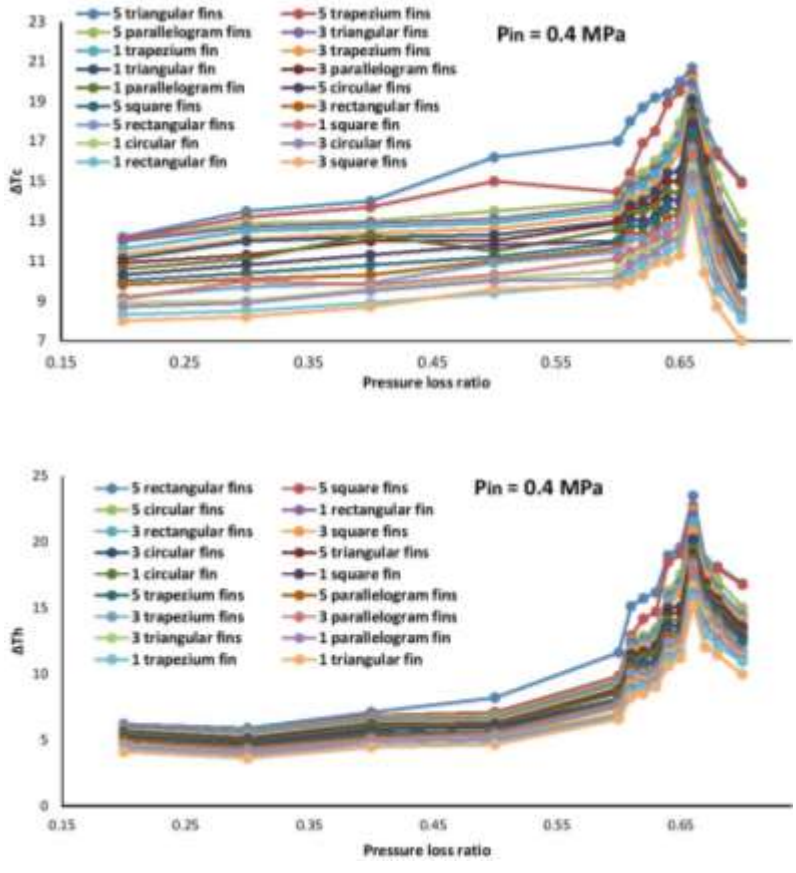

Figure 7 (b) cold and hot temperature difference at Pin = 0.4 MPa.

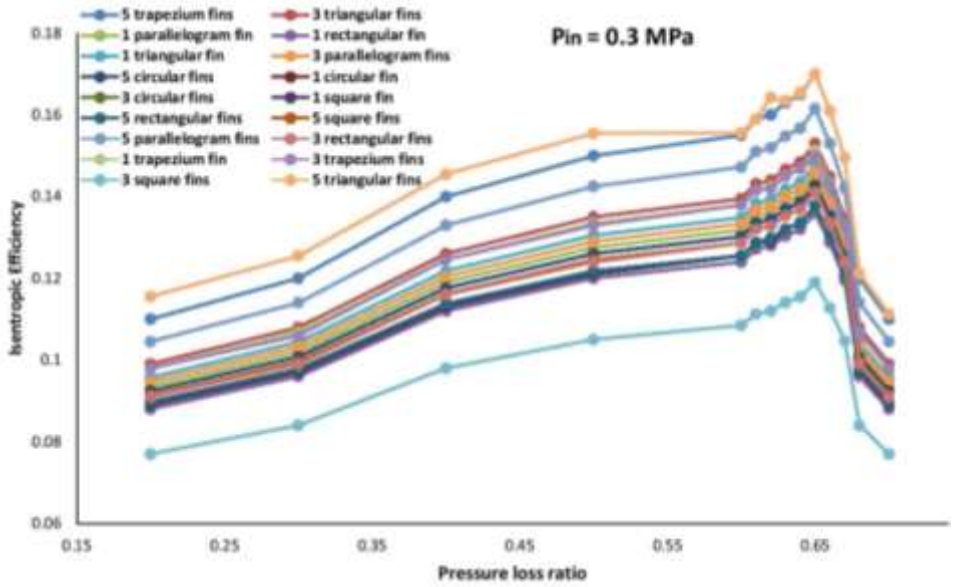

Figure 8 (a) Isentropic efficiency at Pin = 0.3 MPa.

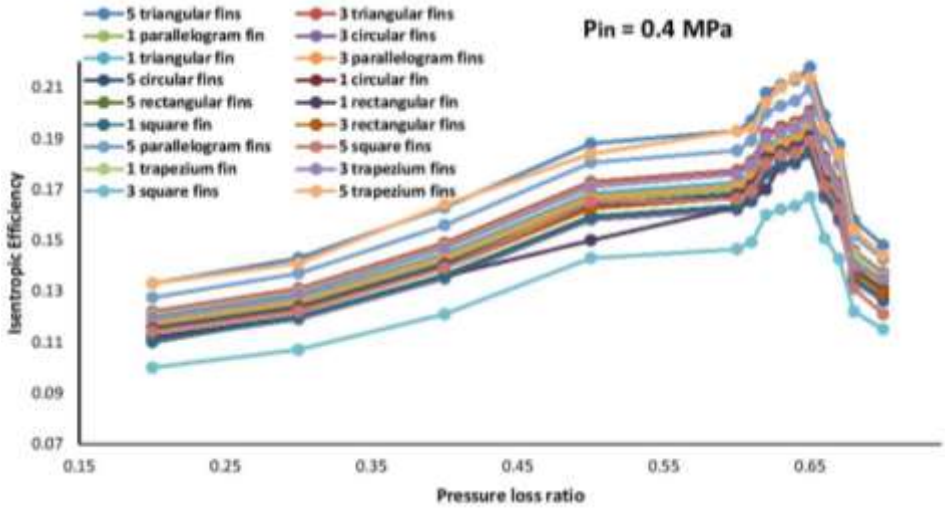

Figure 8 (b) Isentropic efficiency at Pin = 0.4 MPa.

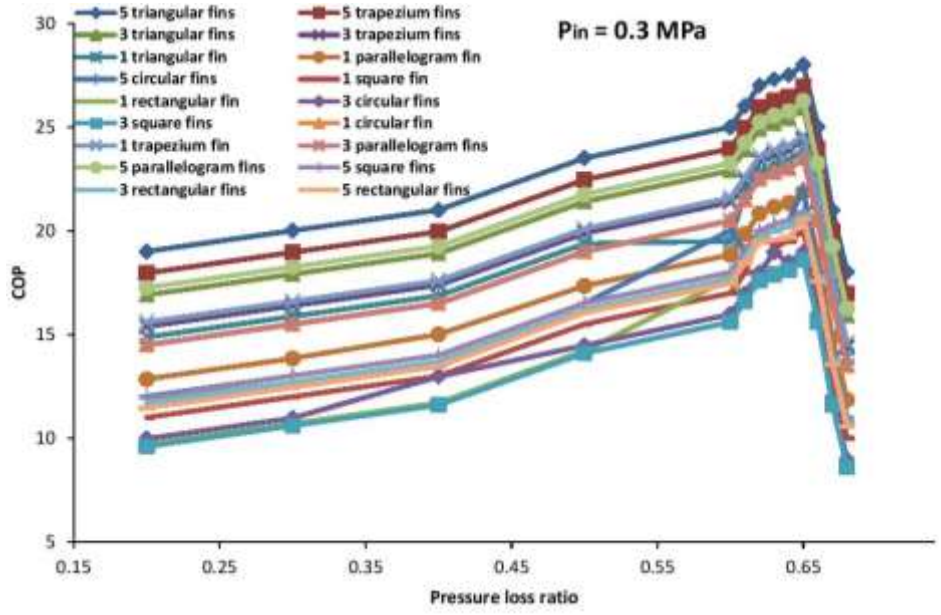

Figure 9 (a) COP at Pin = 0.3 MPa.

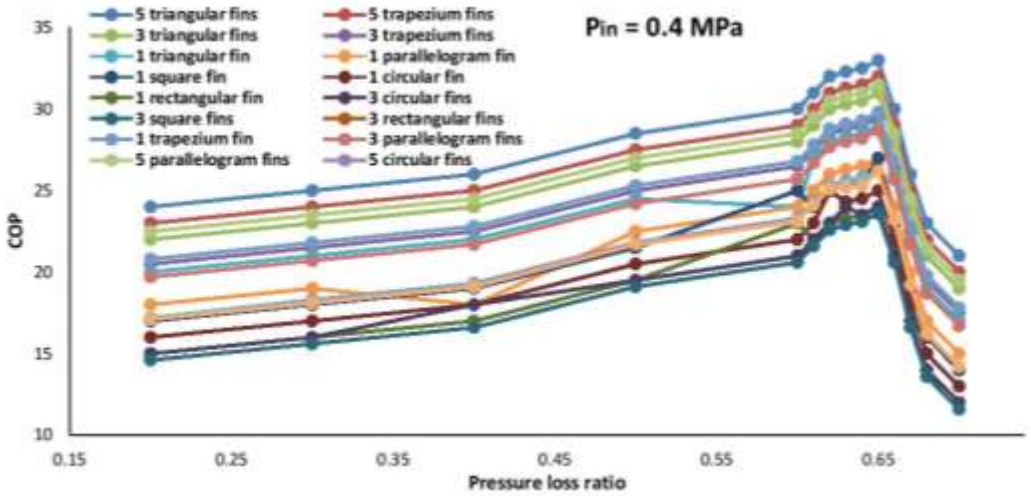

Figure 9 (b) COP at Pin = 0.4 MPa.

difference as shown by equation (5). It is clear that the greatest isentropic efficiency belongs to λ=0.66 as highest cold temperature difference occurs at the same point. Increase in pressure loss ratio beyond λ= 0.66, results in significant isentropic efficiency reduction.

The results show that the isentropic efficiency of the vortex tube with 5 triangular fins is higher than the other ones. This shows that the energy separation has a strong variation with density variation of flow inside the vortex tube. It has been shown that the density gradient for the vortex tube with 5 triangular fins is more than the other cases. This will lead to a higher centrifugal force from which is the main driver for the energy separation. The COP quantities of vortex tubes are indicated at P_in= 0.3 and 0.4 MPa in Fig. 9 (a, b) respectively. In all range of λ, the vortex tube with 5 triangular fins has higher COP values than the other vortex tubes at the same pressure inlet. Similar to isentropic efficiency, COP is directly related to cold temperature difference according to equation (6) and thus The greatest COP is in about λ=0.66 and in range λ > 0.66, the COP value is reduced and results recommend that the COP of the device with 5 triangular fins is greater with respect other kinds of vortex tube, which indicates that the density gradient of the fluid has strong effect on performance since as density increases, causes a stronger centrifugal force. The stronger centrifugal force causes better energy separation as it observed with the vortex tube with 5 triangular fins.

6. CONCLUSIONS

Because vortex tube is economically efficient and environmentally-friendly it can be optimized to be replaced with environment contaminating cooling devices. We present a novel method to investigate the effect of fin installation on the hot tube and to compare the cooling performance of the various vortex tubes. The three-dimensional model is utilized to examine the affection of fin structure on the device performance. The accuracy of CFD result is verified by comparison with the prior available experimental data in the literature. The results show the fin installation on the hot-tube causes different cold air temperature differences and thermal efficiencies for the system. The total and tangential velocity components of the flow are calculated numerically. The research illustrates that the temperature distribution profile varies remarkably after their stagnation points and it was observed that in vortex tube with 5 triangular fins is higher than the other vortex tubes. The result also indicates that the COP and the isentropic efficiency of the device with 3 square fins are less than the other geometries at various pressure loss ratio since a stronger density is stratified from the entrance to the hot end inside the 3 square fins case. Flow behavior within the device illustrates that the flow within the vortex tube consists of only forced and free vortex regimes. The possibility of obtaining the minimum cold temperature always involved the researchers and thus isentropic efficiency involves vortex tubes with installed fins on a hot tube. Efficiency is increased by an increase in cold core flow thickness. Results show that the highest cold temperature difference occurs at λ=0.66; Resulting in greatest efficiency at λ=0.66. The highest vortex tube COP similarly occurred at λ=0.66 as a vortex tube cooler.

Nomenclature	
CFD	Computational Fluid Dynamics
C_p	Heat capacity ($J.kg^{-1}.K^{-1}$)
$C_{\varepsilon i}$	Constant coefficients used in ε equation
C_μ	Constant (equation 15)
C_v	Constant (equation 9)
D	Diameter of vortex tube (mm)
d	Cold outlet diameter (mm)
E	Total energy (kJ)
G_k	Turbulence kinetic energy Production
K_e	Thermal conductivity ($W.m^{-1}.K^{-1}$)
k	Turbulence kinetic energy ($m^2.s^{-2}$)

L	Length (mm)
Ma	Mach number
$\dot{m}$	Mass flow rate ($kg.s^{-1}$)
N	Inlet nozzles number
P	Absolute pressure (Pa)
Pr_t	Turbulent Prandtl number
RNG	Renormalized Group
R	Ideal gas constant (J/kgmol-K)
s	Twice the strain rate tensor (s^{-1})
S_h	Energy fount
T	Temperature (K)
$\Delta T_c = T_{in} - T_C$	cold temperature difference
u_i	i-component velocity magnitude (m/s)
Y_M	Contribution of the fluctuating dilatation
Greek symbols	
α_k	Inverse effective Prandtl numbers for k equation in Eq.7
α_ε	Inverse effective Prandtl numbers for ε equation in Eq.8
δ_{ij}	Kronecker delta
τ	Shear stress ($N.m^{-2}$)
$(\tau_{ij})_{eff}$	Deviatoric stress tensor ($N.m^{-2}$)
ε	Eddy dissipation rate ($m^{-2}.s^{-3}$)
ξ	Fraction of cold mass
μ	Dynamic viscosity ($kg.m^{-1}.s^{-1}$)
υ	Kinematic viscosity ($m^2.s^{-1}$)
$\hat{\upsilon}$	Effective viscosity to the dynamic viscosity ratio
γ	Specific heat ratio
ρ	Density ($kg.m^{-3}$)
η_0, β, η	RNG k- ε model constant coefficients
η_{is}	Isentropic efficiency

Subscripts	
a	Atmospheric
c	Cold fluid
eff	Effective
h	Hot fluid
in	Inlet fluid
is	Isentropic
i , j ,k	Components of Cartesian coordinate
n	Nozzle
st	Static
t	Turbulent

CONFLICT OF INTEREST

The authors declare no conflicts of interest

ACKNOWLEDGEMENTS

This paper was partially supported by Petroleum University of Technology (PUT) organization, Department of gas engineering of (PUT).

REFERENCES

[1]. G. Ranque. Experiments on Expansion in a Vortex with Simultaneous Exhaust of Hot and Cold Air," Le Journal De Physique et le Radium (Paris) 1933; 4: 112-4.

[2]. R. Hilsch. Die expansion von Gasen im Zentrifugalfeld als Kälteprozess, Zeitschrift für Naturforschung A 1946;1:208-14.

[3]. P. P. Edwards, V. L. Kuznetsov, W. I. David, and N. P. Brandon. Hydrogen and fuel cells: towards a sustainable energy future, Energy policy 2008;36:4356-62.

[4]. M. Momirlan and T. N. Veziroglu. The properties of hydrogen as fuel tomorrow in sustainable energy system for a cleaner planet, International journal of hydrogen energy 2005; 30: 795-802.

[5]. D. Pant, A. Singh, G. Van Bogaert, S. I. Olsen, P. S. Nigam, L. Diels, et al. Bioelectrochemical systems (BES) for sustainable energy production and product recovery from organic wastes and industrial wastewaters, Rsc Advances 2012; 2 : 1248-63.

[6]. P. Poizot and F. Dolhem. Clean energy new deal for a sustainable world: from non-CO 2 generating energy sources to greener electrochemical storage devices, Energy & Environmental Science 2011; 4: 2003-19.

[7]. K. Srirangan, L. Akawi, M. Moo-Young, and C. P. Chou. Towards sustainable production of clean energy carriers from biomass resources, Applied energy 2012; 100: 172-86.

[8]. S. Eiamsa-ard and P. Promvonge. Review of Ranque–Hilsch effects in vortex tubes, Renewable and sustainable energy reviews 2008; 12: 1822-42.

[9]. S. Subudhi and M. Sen, Review of Ranque–Hilsch vortex tube experiments using air, Renewable and sustainable energy reviews 2015; 52:172-8.

[10]. T. K. Sharma, G. A. P. Rao, and K. M. Murthy. Numerical Analysis of a Vortex Tube: A Review, Archives of Computational Methods in Engineering 2017; 24: 251-80.

[11]. U. Behera, P. Paul, S. Kasthurirengan, R. Karunanithi, S. Ram, K. Dinesh, et al.CFD analysis and experimental investigations towards optimizing the parameters of Ranque–Hilsch vortex tube, International Journal of Heat and Mass Transfer 2005; 48: 1961-73.

[12]. N. Aljuwayhel, G. Nellis, and S. Klein. Parametric and internal study of the vortex tube using a CFD model, International journal of refrigeration 2005; 28: 442-50.

[13]. E. Smith and P. Pongjet. Numerical prediction of vortex flow and thermal separation in a subsonic vortex tube, Journal of Zhejiang University-SCIENCE A 2006; 7: 1406-15.

[14]. T. Farouk and B. Farouk. Large eddy simulations of the flow field and temperature separation in the Ranque–Hilsch vortex tube, International Journal of Heat and Mass Transfer 2007; 50: 4724-35.

[15]. T. Farouk, B. Farouk, and A. Gutsol. Simulation of gas species and temperature separation in the counter-flow Ranque–Hilsch vortex tube using the large eddy simulation technique, International Journal of Heat and Mass Transfer 2009; 52: 3320-33.

[16]. X. Liu and Z. Liu, Investigation of the energy separation effect and flow mechanism inside a vortex tube, Applied thermal engineering 2014; 67: 494-506.

[17]. F. User's Guide. 6.3 Documentation, Fluent Inc., Lebanon, NH, (2006)
[18]. D. Choudhury. Introduction to the renormalization group method and turbulence modeling: Fluent Incorporated;1993.
[19]. S. Sarkar and L. Balakrishnan, Application of a Reynolds stress turbulence model to the compressible shear layer, in 21st Fluid Dynamics, Plasma Dynamics and Lasers Conference 1990: 1465.
[20]. F. Fluent, 6.3 user's guide, Fluent Inc 2006.